HIGH-ENERGY EMISSION FROM THE TeV BLAZAR MARKARIAN 501 DURING MULTIWAVELENGTH OBSERVATIONS IN 1996

J. KATAOKA,[1,2] J. R. MATTOX,[3] J. QUINN,[4] H. KUBO,[5] F. MAKINO,[1] T. TAKAHASHI,[1] S. INOUE,[6] R. C. HARTMAN,[7]
G. M. MADEJSKI,[7,8] P. SREEKUMAR,[7,9] AND S. J. WAGNER[10]

ABSTRACT

We present the results of a multiwavelength campaign for Mrk 501 performed in 1996 March with *ASCA*, EGRET, Whipple, and optical telescopes. The X-ray flux observed with *ASCA* was 5 times higher than the quiescent level and gradually decreased by a factor of 2 during the observation in 1996 March. In the X-ray band, a spectral break was observed around 2 keV. We report here for the first time the detection of high-energy γ-ray flux from Mrk 501 with EGRET with 3.5 σ significance ($E > 100$ MeV). Higher flux was also observed in 1996 April–May, with 4.0 σ significance for $E > 100$ MeV and 5.2 σ significance for $E > 500$ MeV. The γ-ray spectrum was measured to be flatter than most of the γ-ray blazars. We find that the multiband spectrum in 1996 is consistent with that calculated from a one-zone synchrotron self-Compton (SSC) model in which X-rays are produced via synchrotron emission and γ-rays are produced via inverse Compton scattering of synchrotron photons in a homogeneous region. The flux of TeV γ-rays is consistent with the predictions of the model if the decrease of the Compton scattering cross section in the Klein-Nishina regime is considered. In the context of this model, we investigate the values of the magnetic field strength and the beaming factor allowed by the observational results. We compare the 1996 March multiwavelength spectrum with that in the flare state in 1997 April. Between these two epochs, the TeV flux increase is well correlated with that observed in keV range. The keV and TeV amplitudes during the 1997 April flare are accurately reproduced by a one-zone SSC model, assuming that the population of synchrotron photons in 1996 are scattered by newly injected relativistic electrons having maximum energies of $\gamma_{max} \sim 6 \times 10^6$. However, the TeV spectrum observed during the 1996 March campaign is flatter than predicted by our models. We find that this cannot be explained by either higher order Comptonization or the contribution of the "seed" IR photons from the host galaxy for the first-order external radiation Comptonization, but we cannot exclude possible effects of the IR photons that may arise in the parsec-size tori postulated to exist in active galactic nuclei.

Subject headings: BL Lacertae objects: individual (Markarian 501) — gamma rays: observations — radiation mechanisms: nonthermal — X-rays: galaxies

1. INTRODUCTION

Observations by the EGRET instrument (30 MeV–30 GeV; Thompson et al. 1993) onboard the *Compton Gamma Ray Observatory* (*CGRO*) reveal that γ-ray emission dominates the apparent power output for many blazar type active galactic nuclei (AGNs). About 50 sources detected with EGRET in the high-energy γ-ray band are identified with blazars (see, e.g., Mattox et al. 1997b; Mukherjee et al. 1997). The γ-ray emission extends up to TeV energies for

three nearby blazars: Mrk 421 ($z = 0.031$; Punch et al. 1992; Petry et al. 1996), Mrk 501 ($z = 0.034$; Quinn et al. 1996; Bradbury et al. 1997; Aharonian et al. 1997), and 1ES 2344+514 ($z = 0.044$; Weekes et al. 1996; Catanese et al. 1998).

The overall electromagnetic spectra of blazars, when plotted in the νF_ν space, generally reveal two broad peaks; one located between IR and X-rays, and another in the γ-ray regime (e.g., von Montigny et al. 1995); in a few objects, additional components are observed in the IR/optical band, but those are probably not directly associated with the blazar phenomenon; they are instead likely to be due to the isotropic emission of the associated AGN (e.g., Falomo et al. 1993). The models invoked to explain why the radiative processes in blazars have these two components correspond to two different emission processes from the same population of relativistic particles. The polarization observed in the radio and optical bands indicates that the lower energy emission is most likely due to the synchrotron process, while the inverse Compton mechanism is thought to be dominant for the high-energy γ-ray emission (see, e.g., Ulrich, Maraschi, & Urry 1997). However, the source of the "seed" photons for the Compton process is a matter of debate. In some models, e.g., the synchrotron self-Compton (SSC) model (Jones, O'Dell, & Stein 1974; Marscher 1980; Königl 1981; Marscher & Gear 1985; Ghisellini &

[1] Institute of Space and Astronautical Science, 3-1-1 Yoshinodai, Sagamihara, Kanagawa 229-8510, Japan.

[2] Department of Physics, University of Tokyo, 7-3-1 Hongo, Bunkyo-ku, Tokyo 113-0033, Japan.

[3] Astronomy Department, Boston University, 725 Commonwealth Avenue, Boston, MA 02215.

[4] Fred Lawrence Whipple Observatory, Harvard-Smithsonian Center for Astrophysics, P. O. Box 97, Amado, AZ 85645-0097.

[5] The Institute of Physical and Chemical Research, 2-1 Hirosawa, Wako, Saitama 351-0198, Japan.

[6] Department of Physics, Tokyo Metropolitan University, 1-1 Minami-Osawa, Hachioji, Tokyo, Japan 192-0397.

[7] Laboratory for High Energy Astrophysics, NASA/GSFC, Greenbelt, MD 20771.

[8] Deptartment of Astronomy, University of Maryland, College Park, MD 20742.

[9] Universities Space Research Association.

[10] Landessternwarte Heidelberg, Königstuhl, D-69117 Heidelberg, Germany.

Maraschi 1989; Maraschi, Ghisellini, & Celloti 1992; Marscher & Travis 1996), it is synchrotron radiation internal to the jet, while in others, e.g., the external radiation Compton (ERC) model (Dermer & Schlickeiser 1993; Sikora, Begelman, & Rees 1994) it is radiation external to the jet .

Blazars are highly variable from radio to γ-ray bands: flares with timescales as short as 15 minutes have been observed in the TeV range (Gaidos et al. 1996). The correlation of variability between different bands can potentially discriminate between various models. The first TeV blazar that was observed simultaneously in multiple bands from radio to TeV γ-rays is Mrk 421. The first campaign, conducted in 1994 (Macomb et al. 1995), revealed correlated variability between the keV X-ray and TeV γ-ray emission, where the γ-ray flux varied by an order of magnitude on a timescale of 2 days and the X-ray flux was observed to double in 12 hr. On the other hand, the high-energy γ-ray flux observed by EGRET, as well as the radio and UV fluxes, showed less variability than the keV or TeV bands. Another Mrk 421 multiwavelength campaign performed in 1995 revealed another coincident keV/TeV flare (Buckley et al. 1996; Takahashi et al. 1996b). Although the relative amplitudes of variability are different, the UV and optical bands also showed correlation during the flares. These results indicate that the high-energy tail of the energy distribution of a single electron population is responsible for both the X-rays and TeV γ-rays (Takahashi et al. 1996a). With the detection of TeV emission from Mrk 501 (Quinn et al. 1996), several multiband campaigns were organized to observe this object to verify whether such a behavior is a general property of TeV-emitting blazars or whether it is unique to Mrk 421.

During the 1997 April multiwavelength campaign for Mrk 501, both X-rays and TeV γ-rays increased by more than 1 order of magnitude from quiescent level (Catanese et al. 1997; Pian et al. 1998). While the synchrotron emission peaked below 0.1 keV in the quiescent state, in 1997 it peaked at ~ 100 keV—the largest shift ever observed for a blazar (Pian et al. 1998); this is in contrast to Mrk 421, which shows relatively little variability of the position of the synchrotron peak (e.g., Macomb et al. 1995). Mastichiadis & Kirk (1997) suggest that the SSC scheme in a homogeneous region is sufficient to interpret the multiband spectrum of Mrk 421. They also suggest that the flare in 1994 is probably caused by a change in the maximum energy of electrons (γ_{max}). The origin of the 1997 April flare of Mrk 501 was also investigated by Pian et al. (1998). They calculated that the variation of the γ_{max} together with an increased luminosity and a flattening of the injected electron distribution can describe observed spectra well. Their model shows good agreement with the data, but does not reproduce the TeV γ-ray flux during the high state in 1997 April.

The correlation between the high-energy γ-ray and other bands is important for studying the radiation mechanisms of blazars. A combined GeV and TeV spectrum can place a strong limit on the high-energy emission and its relation with the low-energy emission. However, observations of high-frequency–peaked BL Lac objects (HBLs) in the high-energy γ-ray band from 30 MeV to several GeV are difficult, because HBLs are faint in this energy band (e.g., Mukherjee et al. 1997). For instance, Mrk 421 is detected at a level comparable to the EGRET sensitivity (Fichtel et al. 1994; Thompson et al. 1995). Catanese et al. (1997) present an

EGRET observation of Mrk 501 during the 1997 X-ray/TeV flare (Apr. 9–15), and report a 1.5 σ excess at the position of the source and furnish an upper limit.

In this paper we present Mrk 501 data from simultaneous 1996 March observations by $ASCA$ (keV), EGRET (GeV) and Whipple (TeV), together with the optical observations. The EGRET observation during this campaign indicates a detection with 3.5 σ significance ($E > 100$ MeV) during a 3.2 day interval of peak flux. Also, a month later, EGRET detected Mrk 501 with 4.0 σ significance ($E > 100$ MeV; 5.2 σ for $E > 500$ MeV). This is the first report of the detection of Mrk 501 by EGRET. The observations and analysis are presented in § 2. The multifrequency spectra during the campaign are described and compared with the 1997 April flare state and a quiescent state in § 3. We discuss the radiation mechanism of TeV blazar Mrk 501 in § 4, and present our conclusions in § 5.

2. OBSERVATIONS AND RESULTS

2.1. ASCA

We observed Mrk 501 four times with $ASCA$ during the period 1996 March 21.3–April 2.9 UT. Each pointing was about 10 ks in duration. The observations were performed in a nominal, 1 CCD mode for the Solid-state Imaging Spectrometer (SIS: Burke et al. 1991), and a nominal PH mode for the Gas Imaging Spectrometer (GIS: Ohashi et al. 1996). We applied standard screening procedures to the data and extracted the counts from a circular region centered on the target with a radius of 3′ and 6′ for SIS and GIS, respectively. We used standard blank sky observations to estimate the background. The SIS light curves of these four observations are shown in Figure 1. The count rate includes the background of ~ 0.01 counts s^{-1}. The flux
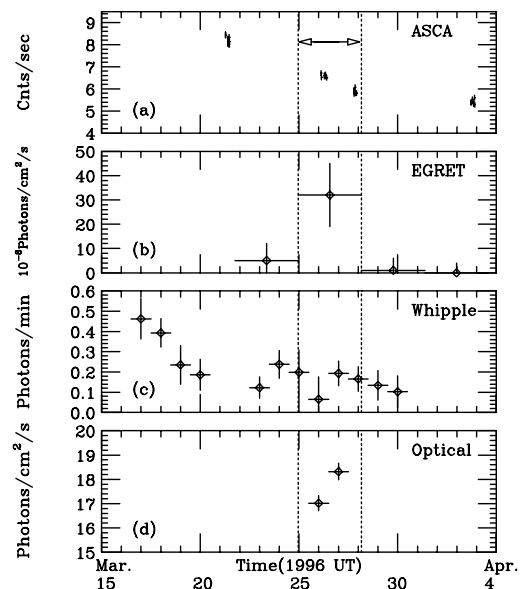

Fig. 1.—Time history of Mrk 501 during the 1996 March campaign: (a) X-ray ($ASCA$: 0.7–10 keV), (b) GeV (EGRET: 100 MeV–10 GeV), (c) TeV (Whipple: above 350 GeV), and (d) Optical (R-band: 650 nm). The $ASCA$ count rates are from the summed SIS0 and SIS1 data, extracted from a circular region centered on the target with a radius of 3′. The time interval marked with arrows is when EGRET detected Mrk 501 at 3.5 σ significance for the first time. All errors are 1 σ.

change between the observations 2 and 3 indicates variability on a timescale of about a day. The flux calculated from the spectrum decreased by a factor 2 over 2 weeks. No evidence was found for time variability within each of the four observations; the maximum χ^2 probability of variability was less than 97%.

We summed all photons detected with both SISs into a single spectrum for each observation, because the hardness ratio (defined as the ratio of counting rates at 1.5–7.5 keV to those at 0.7–1.5 keV) did not change significantly. Here we do not use the GIS data, since the efficiency of GISs in the low-energy band ($E < 2$ keV) is worse than that for SIS and is thus of less utility in a study of details of the spectral shape at low energies; furthermore, for this bright source and a relatively simple model, with SISs alone, we probably reached the level where the statistical errors are comparable to the systematic errors. We first fitted such combined SIS spectra (one per observation) with a single power law with photoelectric absorption whose column density N_H was fixed at Galactic value, 1.73×10^{20} cm^{-2} (Elvis et al. 1989). However, this model did not represent any of the four spectra adequately; a power law fitting the data above 2 keV was too steep for the data below 2 keV. All the SIS data for these four observations showed such discrepancy that the reduced χ^2 ranged from 1.6 to 2.0 for more than 300 degrees of freedom (dof). The single power-law model is thus rejected with higher than 99% confidence level.

A better fit was obtained using a broken power-law model with Galactic absorption, where the spectrum is harder below the break. Even with this more complex model, we observe a clear spectral variability from one observation to another. As summarized in Table 1, the spectrum steepened as the flux decreased from (9.24 ± 0.05) to $(4.21 \pm 0.03) \times 10^{-11}$ ergs cm^{-2} s^{-1} in 2–10 keV. The photon index (Γ_1) below the break energy (E_B) changed from 1.72 ± 0.08 to 1.89 ± 0.08, while the index (Γ_2) above E_B changed from 2.15 ± 0.02 to 2.46 ± 0.03. But the difference $\Gamma_2 - \Gamma_1$ was roughly constant, ~ 0.5, for all periods. Although we do not use GIS data for the above fits, the parameters derived here are consistent when we used both GIS2 and GIS3 data.

Figure 2 shows the correlation between the X-ray flux and the photon index. The maximum flux observed with $ASCA$ was 5 times higher than the quiescent level observed with $Ginga$ (Makino, Fink, & Clavel 1991) and one-fifth of the highest flux ever observed (Pian et al. 1998). As shown in Figure 2, the X-ray spectrum tends to steepen as the source gets fainter. This is a general feature of HBL spectra (see, e.g., Giommi et al. 1990). The spectral break around 2 keV was observed with both $ASCA$ and $BeppoSAX$ (Pian et al.
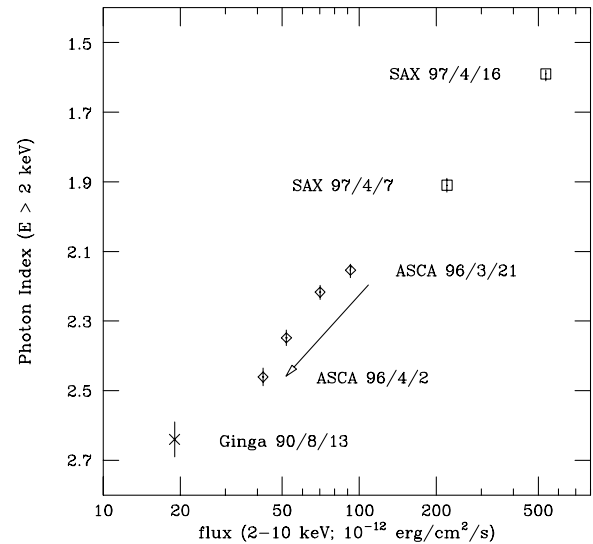

Fig. 2.—Correlation between 2–10 keV flux and spectral photon index above 2 keV for Mrk 501. $Ginga$ and $BeppoSAX$ results are from Makino et al. (1991) and Pian et al. (1998), respectively. All errors are 1 σ. The arrow indicates an evolution during the $ASCA$ observation in 1996 March–April.

1998), while no spectral break was seen in the simultaneous $ROSAT$ PSPC and $Ginga$ observation when the combined 0.1–20 keV spectrum was well described by a power law with the photon index of 2.63 (Makino et al. 1991).

2.2. EGRET

We report here new EGRET results for Mrk 501 for which no EGRET detection has been reported previously. We have performed likelihood analyses (Mattox et al. 1996) of all viewing periods (VP) with exposure greater than 8×10^7 cm^2 s for γ-ray energies $E > 100$ MeV; the results are shown in Table 2. Contributions from diffuse high-latitude galactic emission and extragalactic emission (Sreekumar et al. 1998) were incorporated in the analysis. Note that for VP 519.0 the result is a 4.0 σ detection, barely meeting the acceptance criterion used in the construction of EGRET catalogs (Thompson et al. 1995).

At this point, considerable caution is required because of the large size ($\sim 5°$) of the EGRET point-spread function (PSF), and, in this instance, because of possible source confusion. Within 5° of Mrk 501 are three flat spectrum radio quasars: 3C 345 and NRAO 512, neither of which have ever been convincingly detected by EGRET but which are other-

TABLE 1

Fit Results of $ASCA$ Spectrum

Observaton ID	UT (1996)	Γ_1[a]	E_B[a]	Γ_2[a]	Flux[b]	$\Gamma_2 - \Gamma_1$	χ^2/(dof)
1	Mar 21.26–21.50	1.72 ± 0.02	1.72 ± 0.08	2.15 ± 0.02	9.24 ± 0.05	0.43 ± 0.03	1.00 (379)
2	Mar 26.12–26.42	1.77 ± 0.03	1.67 ± 0.08	2.22 ± 0.02	7.03 ± 0.04	0.45 ± 0.04	0.92 (360)
3	Mar 27.70–27.95	1.89 ± 0.03	1.67 ± 0.07	2.35 ± 0.02	5.20 ± 0.03	0.46 ± 0.04	1.04 (329)
4	Apr 2.69–2.93	1.89 ± 0.03	1.65 ± 0.07	2.46 ± 0.03	4.21 ± 0.03	0.57 ± 0.04	1.04 (313)

Note.—All errors are 1 σ.

[a] Fit model is broken power law with Galactic absorption. Γ_1 and Γ_2 are photon indices in lower and higher energy band, respectively. E_B is break energy in keV. SIS0 and SIS1 data are combined.

[b] 2–10 keV flux in units of 10^{-11} ergs cm^{-2} s^{-1}.

TABLE 2
EGRET RESULTS FOR MRK 501

Viewing Period	Interval	Aspect[a]	Exposure[b]	Significance (σ)	Flux[c]
9.5	1991 Sep 12–19	3.3	2.28	0.5	<11
201.0............	1992 Nov 17–24	2.5	1.12	1.7	9 ± 6
202.0............	1992 Nov 24–Dec 01	5.8	1.06	1.1	8 ± 7
516.5............	1996 Mar 21– Apr 03	3.1	1.47	2.1	10 ± 5
	(1996 Mar 25–Mar 28)		0.46	3.5	32 ± 13
519.0............	1996 Apr 23–May 07	1.2	2.10	4.0	18 ± 5
			2.97	5.2	6 ± 2[d]
617.8............	1997 Apr 04–15	3.0	0.82	1.5	9 ± 7

[a] Angle between the source and the EGRET instrument axis in units of degree.
[b] Exposure in unit of 10^8 cm² s.
[c] Flux ($E > 100$ MeV) in units of 10^{-8} cm⁻² s⁻¹. All errors are 1 σ.
[d] Flux ($E > 500$ MeV) in units of 10^{-8} cm⁻² s⁻¹. All errors are 1 σ.

wise similar to the highly variable EGRET-detected quasars; and 4C +38.41, which has been detected several times by EGRET, and at times has been very bright. To verify that the source detected in VP 519.0 really was Mrk 501, an analysis was done for $E > 500$ MeV. Although the number of photons detected above 500 MeV is considerably smaller than above 100 MeV, the extent of the PSF for the higher energy photons is reduced by a factor of about 6 in solid angle, enough to remove the possibility of confusion with the other nearby objects. The result of the $E > 500$ MeV analysis is a 5.2 σ detection and source location contours (Fig. 3) that clearly pinpoint Mrk 501 as the source of the γ-ray emission. The strong $E > 500$ MeV detection suggests a very hard spectrum, and indeed, spectral analysis gives a photon spectral index of 1.3 ± 0.5, one of the hardest spectra ever determined with EGRET.

The VP 516.5 & 519.0 observations listed in Table 2 have been examined for a possible time variability. A Kolmogorov-Smirnov (KS) test of the cumulative number of events (with $E > 70$ MeV) from the direction of Mrk 501 as a function of time has been performed (as described by Mattox et al. 1997a). For the 1996 March 21–April 3 EGRET observation (which coincides with the *ASCA* observation described in § 2.1), Kuiper's variant of the KS test (Press et al. 1992) indicates variability with 98.9% confidence. This interval was therefore analyzed through a likelihood analysis of four equal length intervals with $E > 100$ MeV. The light curve thus produced is shown in Figure 1. The second subinterval, 1996 March 24.96–28.17, showed a detection significance of 3.5 σ and a flux of $(32 \pm 13) \times 10^{-8}$ cm⁻² s⁻¹, $E > 100$ MeV. The spectral photon index was measured to be 1.6 ± 0.5 in the 30 MeV–10 GeV energy range during the 1996 March 24.96–28.17 subinterval. A χ^2 test of variability using the fluxes of these four intervals indicates variability with 88% confidence. From Figure 1, a correlation with the TeV flux appears plausible, but the EGRET statistics are too sparse for a definitive evaluation. For the 1996 April 23–May 7 exposure, Kuiper's variant of the KS test indicates variability with 95% confidence. Higher flux is indicated between 1996 April 23.88 and 29.13 and between 1996 May 4.19 and 7.44. For the 1997 April 4–15 exposure, a likelihood analysis finds a 1.5 σ indication of $E > 100$ MeV flux. During this interval, Mrk 501 was observed to flare in the TeV and hard X-ray bands (Catanese et al. 1997; Aharonian et al. 1997; Pian et al. 1998).

For VP 516.5 and VP 617.8, there are not enough photons above 500 MeV to enable an analysis similar to that done for VP 519.0 above 500 MeV. For VP 516.5, the time proximity to the rather strong emission in VP 519.0 suggests that Mrk 501 is probably the source of the 2.1 σ detection, and, particularly, the 3.5 σ detection, in the 3.2 day subinterval of the multiwavelength campaign, especially in view of the TeV activity during that time.

The 1 yr interval between VP 519.0 and VP 617.8 prevents any similar conclusion based on the EGRET data alone; however, the strong TeV activity during VP 617.8 again suggests that Mrk 501 is the source of γ-ray radiation possibly detected by EGRET at that time.

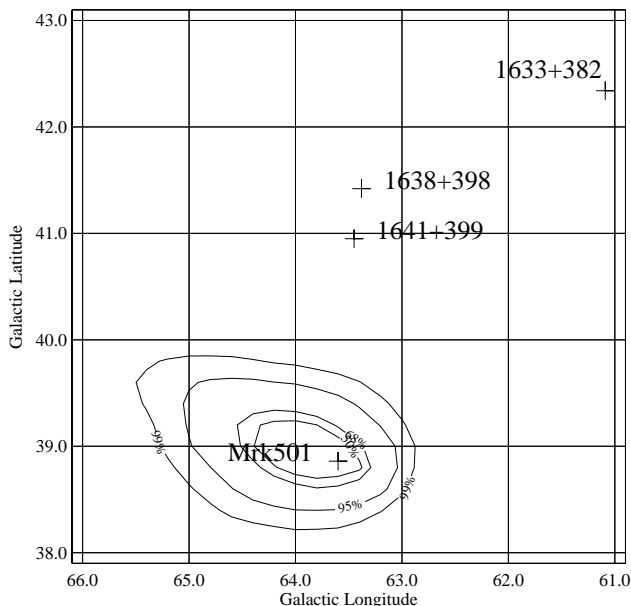

FIG. 3.—Maximum likelihood map of EGRET observations using photons above 500 MeV. The smaller PSF at higher energies yields good positional identification with Mrk 501 while clearly ruling out association with other nearby blazars.

2.3. TeV Observations

Mrk 501 was observed at $E > 350$ GeV with the Whipple Atmospheric Cherenkov Imaging Telescope (Cawley & Weekes 1995) 1996 March 17–30 as a part of the multiband

campaign. The data for the nights of March 21 and 22 were discarded owing to poor weather conditions. The resulting data set comprises 17.5 hr of good-weather observations. The data were analyzed with Tracking analysis, using the γ-ray selection criteria optimized on Crab Nebula data (see, e.g., Quinn et al. 1996). The resulting light curve is shown in Figure 1. The average emission level for the observation period is 0.20 ± 0.03 photons per minute, approximately 15% that of the corresponding rate from the Crab Nebula. This is almost double the average flux level observed from Mrk 501 in 1995 (Quinn et al. 1996). The flux appears to be highest on the first night of observation $(0.46 \pm 0.10$ photons per minute), and then decreases over a period of a couple of days to a relatively constant level of 0.15 ± 0.03 photons per minute. A χ^2 analysis for constant emission produces a χ^2/dof of $21.5/11$, which indicates variability at the 97% level (a 2.3 σ effect). The χ^2 test was also applied to each night's data to search for evidence of variability within a night: none was found.

According to Petry (1997) (see also Bradbury et al. 1997), HEGRA also observed Mrk 501 from 1996 March 28 to August, partially overlapping our observation. The energy threshold was 1.5 TeV. The photon index of combined spectrum during this 5 months was measured to be 2.5 ± 0.4 (total error) and the average flux was consistent with that of Whipple, measured during our campaign in 1996 March.

2.4. Optical Observations

A few optical observations were carried out using the 70 cm telescope of the Landessternwarte in Heidelberg. Poor weather prohibited strictly simultaneous observations for most of the campaign. It was possible, nevertheless, to obtain a few measurements on 1996 March 26 and 27. Three observations in R-band were taken in both nights, separated by about 1 hr. Since no variability was found within either of the nights within the photometric accuracy of $\sim 1.8\%$, the three frames were co-added and an average flux for each of the nights was derived. The observed magnitude at 650 nm was $m_R = 11.80 \pm 0.02$ for March 26 and $m_R = 11.72 \pm 0.02$ for March 27. The probability of variability in the optical band within the two nights is only 2.3 σ, and hence is not significant. The average brightness in each night is about 30% lower than the average brightness in the R-band measurements from the NED database. Since the absolute fluxes in any optical band depend on the correction for the contribution of the host galaxy and a bit on the effective transmission of standard filters and CCD response, it is not possible to judge whether this difference is due to the source activity or systematic differences.

3. MULTIBAND SPECTRUM

The multiband spectra of Mrk 501 taken during our campaign and at other times are shown in Figure 4. Open circles show the *ASCA*, EGRET, Whipple, and optical data for 1996 March 25–28, when EGRET detected the emission $E > 100$ MeV from Mrk 501 for the first time at 3.5 σ level. The *ASCA* points are determined from a combined fit of data taken during observations 2 and 3. The X-ray flux in the 2–10 keV band was 6.0×10^{-11} ergs cm^{-2} s^{-1}. The TeV count rates observed with Whipple are converted to integral fluxes by scaling them as a multiple of Crab Nebula count rate with the assumption that the photon index is the same as that of Crab, 2.5 (Hillas et al. 1998). The TeV flux plotted in Figure 4 is $(1.23 \pm 0.6) \times 10^{-11}$ photons cm^{-2}
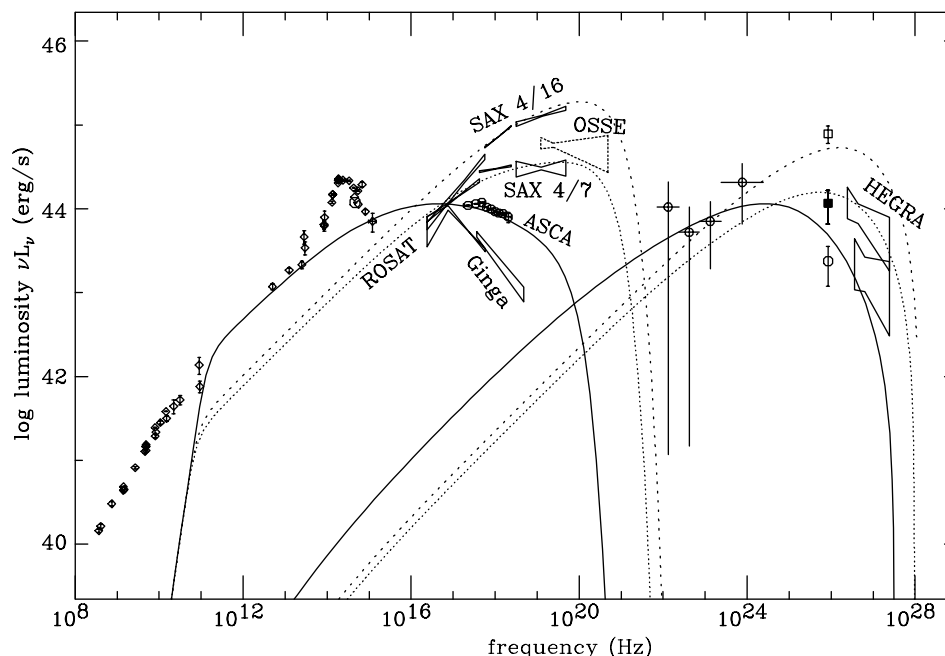

FIG. 4.—Multiband spectrum of Mrk 501. *Circles*: 1996 March 25–28 campaign. *Open squares*: Whipple flux on 1997 April 16. *Filled squares*: Whipple flux on 1997 April 7. *Diamonds*: nonsimultaneous data from the NED database. Sources: *ROSAT* (Comastri et al. 1997), *Ginga* (Makino et al. 1991), *BeppoSAX* (Pian et al. 1998), OSSE (Catanese et al. 1997), EGRET (this work), Whipple (Quinn et al. 1996; Catanese et al. 1997), and HEGRA (Bradbury et al. 1997; Aharonian et al. 1997). The OSSE data are average flux from 1997 April 9–15. The lower HEGRA plots are averages from 1996 March–August, while the upper plots are averages from 1997 March 15–20. Both statistical and systematic errors are included in the HEGRA plots. The solid line corresponds to our model to the spectrum in 1996 March, the dotted line to the data on April 7, and the line with small dashes for 1997 April 16.

s^{-1}, consistent with the flux in 1995, $(0.8 \pm 0.1) \times 10^{-11}$ photons cm^{-2} s^{-1} (Quinn et al. 1996). The optical point is an average value of March 26–27, converted to the energy flux of $(5.40 \pm 0.07) \times 10^{-11}$ ergs cm^{-2} s^{-1}.

In order to know the change of the multifrequency spectra for various phases of source activity, we also plot in Figure 4 the spectra for the pre-1995 quiescent state and the 1997 April flare. Although the X-ray flux observed with *ASCA* was decreasing over a 2 week period, the long-term changes of the X-ray spectra from 1991 (*Ginga*) to 1997 (*BeppoSAX*) suggest that our 1996 March multiwavelength campaign was conducted in the transition phase from the quiescent to the high state. Since a transition of the states in blazars is certainly not smooth or monotonous, the fact that the X-ray flux observed with *ASCA* was decreasing is essentially irrelevant for this interpretation.

The differences in the spectral indices observed with *ASCA* ($\Gamma_2 - \Gamma_1$; see Table 1) show a roughly constant value of ~ 0.5, which is expected from the synchrotron cooling process (e.g., Sikora et al. 1994; Mastichiadis & Kirk 1997). Together with the fact that the peak of the synchrotron emission ordinarily exists near the UV band in the quiescent state (George, Warrick, & Bromage 1988), the spectral break around 2 keV observed with *ASCA*, when the source was in the "intermediate" state, is considered to be the peak of the synchrotron emission. The location of this break increased to ~ 100 keV, when the source was in the high state (Pian et al. 1998). We compare the X-ray and TeV fluxes of three multiwavelength observations: 1996 March 25–28, 1997 April 7, and 1997 April 16. Compared with that in 1996 March, the 2–10 keV flux was higher by a factors of 3.6 on 1997 April 7 and 8.9 on 1997 April 16. The simultaneous increase in the Whipple flux above 350 GeV for these two dates was by factors of 4.9 and 33, respectively. We discuss the amplitude for the correlated variation of the keV and TeV band in the next section.

4. DISCUSSION

During our campaign in 1996 March, a variability of about 30% in the X-ray flux was observed on timescale of a day from Mrk 501. Assuming that the radiation is isotropic and all photons are created in the same region of the size implied by the variability timescale t_{var}, the optical depth to pair production for TeV and keV photons is estimated as $\tau \gtrsim 30$ (e.g., Mattox et al. 1997a), where t_{var} (as measured in the observer's frame) is assumed to be 10^5 s. To avoid absorption of γ-rays due to pair production, current models of blazars assume that the radiation is Doppler-boosted (e.g., Maraschi et al. 1992). We can limit the beaming factor to $\delta \gtrsim 1.9$ (assuming $H_0 = 75$ km s^{-1} Mpc^{-1}). However, a stronger limit should be imposed if there were more rapid flux changes that we could not detect because of our sampling. For instance, during the low state in 1986, an X-ray variability on a timescale of a few hours was observed from Mrk 501 by *EXOSAT* (Giommi et al. 1990). Quinn et al. (1999) also reported variability with a doubling time of 2.5 hr in the TeV band during one flare in 1997 June. Furthermore, there exists evidence of correlated variability in the *U*-band and TeV band during the flare in 1997 April (Catanese et al. 1997). In this case, we can strengthen the limit for the beaming factor to $\delta \gtrsim 6.4$ for t_{var} of 10^4 s.

We apply a one-zone, homogeneous SSC model to the 1996 March multiband data, generally following the prescriptions of Inoue & Takahara (1996). A spherical geometry is adopted, with R being the radius of the emission region. An injection of a power-law energy distribution of electrons up to a certain maximum energy (as expected from shock acceleration) into the radiating region should yield a steady-state electron distribution with a break in its index at a characteristic energy, determined by the balance between radiative cooling and advective escape and/or adiabatic energy loss. (e.g., Sikora et al. 1994; Mastichiadis & Kirk 1997). The resulting synchrotron emission spectrum should reflect this broken power-law form, with the electron index p related to the spectral energy index of the emission α by $\alpha = (p - 1)/2$. What the observed multiband spectrum (Fig. 4) actually suggests is the presence of two breaks in the synchrotron component; one in the IR to optical region and the second in the X-ray band, both with the spectral index changes of ~ 0.5. Moreover, we were unable to adequately fit the whole spectrum including the γ-ray band with a model utilizing an electron distribution with only one break and a maximum energy cutoff. We therefore choose to employ a double broken power-law form for the electron distribution $N(\gamma)$, in which $N(\gamma) \propto \gamma^{-s}$, $\propto \gamma^{-s-1}$, and $\propto \gamma^{-s-2}$ in the energy ranges $\gamma \lesssim \gamma_{b1}$, $\gamma_{b1} \lesssim \gamma \lesssim \gamma_{b2}$, and $\gamma_{b2} \lesssim \gamma \lesssim \gamma_{max}$, respectively. The injection index s is taken to be $s = 2$, and we treat the two break Lorentz factors γ_{b1}, γ_{b2}, and the maximum Lorentz factor γ_{max} as parameters. (The particular form employed in the calculations below, $N(\gamma) \propto \gamma^{-s}(1 + \gamma/\gamma_{b1})^{-1}(1 + \gamma/\gamma_{b2})^{-1}$, was chosen simply for convenience; using sharp breaks instead produces only small changes in the resulting spectrum.) Such a second break (or equivalently, a broad cutoff) in the distribution may effectively result from incorporating a more realistic geometry and/or detailed kinetic evolution of the particle distribution in the downstream region of the shock front (see, e.g., the discussion in Kirk, Rieger, & Mastichiadis 1998). However, deeper inquiry into this is beyond the scope of this paper; it is introduced here only in order to provide a better description of the data.

Synchrotron emission including self-absorption is calculated using the standard spherical solution to the radiative transfer equation,

$$L_{sync}(\nu) = 4\pi^2 R^2 \frac{j_\nu}{\alpha_\nu} \left\{ 1 - \frac{2}{\tau_\nu^2} \left[1 - e^{-\tau_\nu}(\tau_\nu + 1) \right] \right\}, \quad (1)$$

where j_ν and α_ν are, respectively, the emission and absorption coefficients for synchrotron radiation (e.g., Blumenthal & Gould 1970; Gould 1979; Bloom & Marscher 1996). τ_ν is the optical depth in the blob along the line of sight and is expressed as $\tau_\nu = 2\alpha_\nu R$. The electron pitch angle with respect to the magnetic field is set to $\theta = \pi/2$.

We calculate the inverse Compton emission, incorporating the effects of cross section reduction in the Klein-Nishina regime. The differential photon production rate $q(\epsilon)$ is

$$q(\epsilon) = \int d\epsilon_0 \, n(\epsilon_0) \int d\gamma N(\gamma) C(\epsilon, \gamma, \epsilon_0), \quad (2)$$

where ϵ_0 and ϵ are, respectively, the soft photon energy and the scattered photon energy in units of $m_e c^2$, $n(\epsilon_0)$ is the number density of soft photons per energy interval, and $C(\epsilon, \gamma, \epsilon_0)$ is the Compton kernel of Jones (1968). To be exact, $n(\epsilon_0)$ varies depending on the position in the emission blob, and we have to take this effect into account. Approximately, we calculated $n(\epsilon_0)$ at the center of the blob with the

correction factor of $C_{corr} = 0.75$ (Gould 1979). Thus we have

$$n(\epsilon_0) = \frac{4\pi}{hc\epsilon_0} C_{corr} \frac{j_\nu}{\alpha_\nu} (1 - e^{-\alpha_\nu R}),\quad (3)$$

where h is the Planck constant. The convolution in equation (2) is performed under the condition

$$\epsilon_0 \leq \epsilon \leq \gamma \frac{4\epsilon_0 \gamma}{1 + 4\epsilon_0 \gamma}\quad (4)$$

from the kinematics of electron-photon scattering.

We applied this model to the observed spectrum of Mrk 501. To approximate the values for magnetic field and beaming factor, we first place constraints on the allowed parameter space similar to Bednarek & Protheroe (1997), calculated for the case of Mrk 421. In the following prescriptions, we basically assume the parameter space for the 1996 March data. However, because of the lack of the information in the hard X-ray band and the high-energy tail of the TeV spectrum during this campaign, we also use the noncontemporaneous data sets for the calculation.

Since the *Ginga* data in the quiescent state shows no spectral cut off below 20 keV (Fig. 4), it is probable that the synchrotron spectrum in 1996 March also extends above 20 keV. We assume here the maximum synchrotron energy at 50 keV. We thus obtain $\gamma_{max} = 3.2 \times 10^6 B^{-0.5} \delta^{-0.5}$. The Compton-scattered spectrum extending to higher than 10 TeV (Aharonian et al. 1997) gives us the limitation of $\gamma_{max} m_e c^2 \geq 10$ TeV/δ. Using both equations, we can limit the magnetic field to $B \leq 2.6 \times 10^{-2} \delta$ gauss. This limit is represented by line I in Figure 5.

The second constraint is derived using the ratio of the synchrotron and Compton luminosities. Here we can use a relation for the Thomson regime, since the Compton luminosity is well approximated as that for the EGRET range and the high-energy γ-ray spectrum shows no sign of Klein-Nishina cutoff in the MeV–GeV band (Fig. 4). Thus the energy density of the synchrotron radiation u_{sync} is related to the magnetic field density u_B as $u_B = u_{sync} (L_{sync}/L_{SSC})$, where L_{sync} and L_{SSC} is the observed synchrotron/Compton luminosity. Since u_{sync} is represented as

$$u_{sync} = \frac{L_{sync}}{4\pi R^2 c \delta^4},\quad (5)$$

we have the relation

$$u_B = \frac{d_L^2}{R^2 c \delta^4} \frac{l_{sync}^2}{l_{SSC}},\quad (6)$$

where d_L is the luminosity distance, l_{sync} and l_{SSC} are energy flux in observer's frame. From Figure 4, we can approximate l_{sync} and $l_{SSC} \sim 10^{-10}$ ergs cm^{-2} s^{-1}. The upper limit for R is also given as

$$R \leq ct_{var}\delta,\quad (7)$$

where t_{var} is the minimum variability timescale in the observer's frame. Using equations (6) and (7), with t_{var} expressed in seconds, we obtain $B \geq 4 \times 10^6 t_{var} \delta^{-3}$ gauss. This limit is represented by line II in Figure 5.

The third constraint is derived from the evaluation of a variability timescale and synchrotron cooling timescale (t_{sync}). Although the minimum variability timescale must be determined by the balance between radiative cooling and
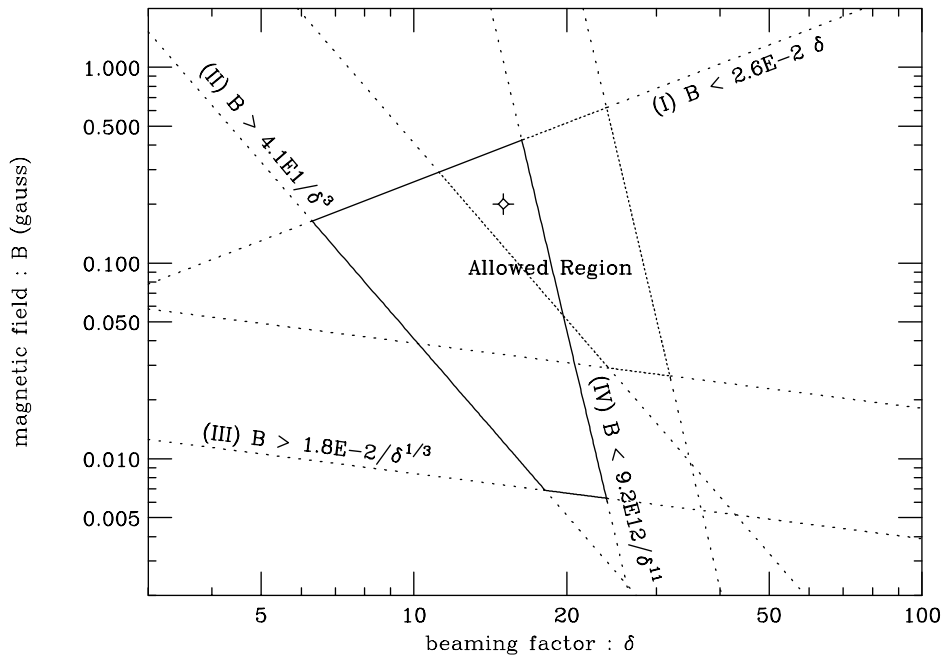

FIG. 5.—Parameter space (B, δ) allowed by the one-zone SSC model for Mrk 501 data. The figure surrounded by the solid line is the allowed parameter space for variability timescale $t_{var} = 10^5$ s, and the cross point is the parameter used for our model (Fig. 4). The figure with dotted lines is the allowed parameter space for $t_{var} = 10^4$ s. Small dashes are constraints from each equations described in § 4 for the case of $t_{var} = 10^5$ s and $t_{var} = 10^4$ s. Line (I) is derived from the maximum energy of synchrotron emission (assumed here to be 50 keV) and Comptonized spectrum ($E > 10$ TeV). Line II is derived from the observed luminosity ratio of the synchrotron and inverse Compton components. Here we used $l_{sync} \sim l_{SSC} \sim 10^{-10}$ ergs cm^{-2} s^{-1}. Line III is derived from the evaluation of the synchrotron cooling time (t_{sync}) and the variability timescale in the jet frame ($t_{var}\delta$). Line IV is derived from the evaluation of the Compton cooling time (t_{SSC}) and the variability timescale in the jet frame. In the process of line I, we utilize noncontemporaneous data. Note that the equation of γ_{max} derived in line I is subsequently used in lines III and IV.

adiabatic energy loss or advective escape (e.g., Sikora et al. 1994; Mastichiadis & Kirk 1997), the synchrotron emission can be one of the most dominant cooling processes; the X-ray spectrum of Mrk 501, which tends to steepen as the source gets fainter, supports this assumption (see Fig. 2). For the electrons of large γ ($\gamma \geq \gamma_{b1}$), t_{sync} is smaller than the source crossing timescale R/c. Combining this with equation (7), we obtain $t_{var}\delta \geq t_{sync}$. Since t_{sync} is represented as

$$t_{sync} = \frac{3m_e c}{4u_B \sigma_T \gamma}, \qquad (8)$$

where σ_T is the Thomson cross section, it becomes minimum at $\gamma = \gamma_{max}$. The lower limit for B is thus calculated as $B \geq 3.9 \times 10 t_{var}^{-2/3} \delta^{-1/3}$ gauss. This limit is represented by line III in Figure 5.

The final constraint is that from the evaluation of the variability timescale and Compton cooling timescale (t_{SSC}). Even for the creation of TeV photons, scatterings in the Thomson regime can be dominant if $\gamma_{max} h\nu < m_e c^2 \delta$ and $\gamma_{max}^2 h\nu > 1$ TeV are satisfied at the same time, where $h\nu$ is the soft photon energy in the observer's frame. These inequalities have a self-consistent solution for $h\nu < \delta^2/4$ eV, under the condition of $B < 5\delta$ gauss. We then approximate t_{SSC} using equation (8), replacing the magnetic field density by the synchrotron photon density. To estimate the value of u_{sync}, $L_{sync} \sim 10^{45}$ ergs s^{-1} is used here. Thus t_{SSC} at $\gamma = \gamma_{max}$ is calculated as $3 \times 10^{-12} t_{var}^2 B^{0.5}\delta^{6.5}$, where we assume R as $ct_{var}\delta$, rather than using inequality (7). This is not true in the strict sense, although it is plausible if t_{SSC} at $\gamma = \gamma_{max}$ is much shorter than $t_{var}\delta$. The previous discussion for $t_{var}\delta \geq t_{sync}$ supports our assumption if $u_B \sim u_{sync}$. The magnetic field is then calculated to be $B \leq 9 \times 10^{22} t_{var}^{-2} \delta^{-11}$ gauss. This limit is represented by line IV in Figure 5.

In Figure 5, we show the allowed values of B as a function of δ for the case of Mrk 501 data sets. These four limits are derived for t_{var} of 10^5 sec, which is observed with ASCA in 1996 March. We also calculate the limits that corresponds to the minimum timescale t_{var} of 10^4 s for more rapid flux changes that we could not detect because of our sampling. The input parameters for our model are determined at the center of the overlapped region for those different timescales: $B = 0.2$ gauss, $\delta = 15$, and $R = 4.5 \times 10^{15}$ cm. The electron distribution is then fixed as: $\gamma_{min} = 1.0$, $\gamma_{b1} = 1.2 \times 10^4$, $\gamma_{b2} = 3.7 \times 10^5$, and $\gamma_{max} = 1.8 \times 10^6$. As shown in Figure 4, the whole spectrum is adequately represented, except for the IR/optical feature near 10^{14} Hz and a discrepancy in the TeV spectrum. One can also see the discrepancy in the radio band, but this can be an effect of at least a part of the emission arising at a larger distance than the location of the keV/TeV emitting region. The one-zone models cannot account for the low-energy emission, which is thought to be produced in a much larger region of the source (e.g., Marscher 1980; see also Pian et al. 1998). However, investigation of this low-energy discrepancy is beyond the scope of this paper; in the following, we concentrate on the discrepancy in the higher energy band, where the one-zone models are thought to be a reasonable approximation to account for the power output of blazars.

The predicted photon index in the HEGRA band is 3.8, while the observed value is 2.5 ± 0.4 (Petry 1997; Bradbury et al. 1997). The photon index in the EGRET energy range (30 MeV–10 GeV) is predicted to be 1.8, which is consistent with the observed value of 1.6 ± 0.5. The rest-frame luminosity is also calculated to be $L'_{sync} = 2.2 \times 10^{40}$ ergs s^{-1} and $L'_{SSC} = 1.8 \times 10^{40}$ ergs s^{-1}. From integration of $\gamma N(\gamma)$, the energy density of relativistic electrons in the source frame is estimated to be 0.16 ergs cm^{-3} and Compton optical depth is $\tau_c = 6.3 \times 10^{-5}$.

It is worthwhile to compare the overall spectrum and the parameters derived by us to those obtained for Mrk 421 (see, e.g., Takahashi et al. 1996a). Observationally, the spectrum of Mrk 421 also shows a spectral break around 1 keV, but its energy does not seem to vary more than a factor of a few when the source enters a flare state, while Mrk 501 shows a change of a factor of ~100. Our modeling indicates that the derived magnetic field B is comparable between the two sources, on the order of 0.2 gauss, but the main difference appears to be the energy of electrons radiating at the peak of the synchrotron component during the flare, γ_{max}, which for Mrk 421 is a few times 10^5 to 10^6, while for the flare of Mrk 501, it is larger, several times 10^6 or greater (e.g., Inoue & Takahara 1996; Pian et al. 1998; see also below). While for Mrk 421 an independent verification of these parameters exists via the comparison of the Klein-Nishina limit to the implications of the spectral variability observed in X-rays (e.g., Mastichiadis & Kirk 1997; Bednarek & Protheroe 1997), we do not have a well-sampled X-ray light curve for Mrk 501, and thus cannot make such a comparison here.

In any case, those large differences indicate that the overall electromagnetic spectra of HBLs are qualitatively similar but peak at different energies, which is likely to be a result of different energy distribution of radiating electrons. Kubo et al. (1998) found that B is similar over a large range of blazar classes, and the difference of the overall spectra— where the blazars associated with quasars (showing emission lines) have synchrotron components peaking in the infrared, as opposed to HBLs, where these peaks are in the X-ray regime—can be also explained by lower γ_{max} in quasar-type blazars than in HBLs. However, it is not possible as yet to determine if this is intrinsic, i.e., related to different conditions for the particle acceleration process, or if some external conditions (such as the strong diffuse radiation field) play an important role in the particle population inferred from the observations.

We next investigate whether the one-zone SSC model might be helpful for understanding the large flare observed in 1997 April. Inspection of Figure 4 suggests that two different components probably contribute to the synchrotron spectrum, one a steady component, and another, variable, responsible for the sudden increase of the highly energetic electrons when the source goes into the flare state. We set γ_{max} to 5.5×10^6 for the April 7 data and 7.0×10^6 for the April 16 data. The parameters such as region size, magnetic field, and beaming factor are the same as that for 1996 March. The normalization was determined from the synchrotron spectra obtained during the BeppoSAX observations (Pian et al. 1998). For these flare data, a single break population of electrons is adequate to account for the multiband spectrum ($\gamma_{b1} \sim \gamma_{b2}$).

We first assumed that the newly injected electrons scatter only the photons emitted by the electron population associated with the flare. However, the calculated flare amplitude of the TeV flux was substantially lower than that observed. We next assumed that there exists a steady population of synchrotron photons, with the same level as that in 1996,

and those are scattered by the flare electron population. In this case, the flare amplitude of the TeV flux is quite well reproduced, as shown in Figure 4. The photon index in the HEGRA region is predicted to be 2.6 for 1997 April 7, comparable with the observational data of $2.49 \pm 0.11 \pm 0.25$ (Aharonian et al. 1997). This result is consistent with Pian et al. (1998), where the scattering of the steady component by the flare electron population is necessary to account for the flare amplitude of the TeV flux. This may imply that the steady and the flare components arise from close parts of the jet and have some interaction with each other. Unfortunately, the observed data during the flare are too sparse to discriminate whether the two emission components originate in the same region or different regions of the jet. More precise observations in various energy bands (and, in particular, better sampling) are necessary to further understand this problem.

The relatively flat shape of the spectrum observed with HEGRA in 1996 March is discrepant with our one-zone model. We investigated two possible causes of this discrepancy. The first is the external soft photons from the host galaxy or an obscuring torus and the other is the multiple Comptonization. The integration of the stellar light from the galaxy can be the origin of the IR/optical feature present around 10^{14} Hz (see Fig. 4; Falomo et al. 1993). These photons are distributed isotropically in the observer's frame and are injected externally into the emission region. The IR photons are important since they can be scattered to TeV energies ($\gamma_{max} \sim 10^6$) without entering the Klein-Nishina regime. Additionally, Comptonization of such external photons can be more effective than SSC, because of the anisotropy of injected photons in the frame of the jet (Sikora et al. 1994; Dermer 1995; Dermer et al. 1997). To account for the flat TeV spectrum with such external radiation, the observed external Compton luminosity (L_{ext}) must be at least comparable with the synchrotron luminosity (L_{sync}). This means that the energy densities of magnetic field and external photons have the relation $u_{ext} \sim u'_{ext}/\delta^2 \gtrsim u_B/\delta^4$, where u_{ext} is the density of external photons in the observer's frame and u'_{ext} in the jet frame. For our model of $B = 0.2$ gauss and $\delta = 15$, we obtain the constraint of $u_{ext} \gtrsim 10^{-8}$ ergs cm^{-3}. The typical values for the total luminosity of the galaxy $L_{gal} = 10^{44}$ ergs s^{-1} and effective radius $R_{eff} = 1$ kpc (e.g., Binney & Tremaine 1987) give the energy density of $u_{ext} \sim 3 \times 10^{-11}$ ergs cm^{-3}—much smaller than the lower limit given above—and thus the galactic IR photons aren't expected to affect the TeV spectrum.

However, if the IR photons arise in a region comparable to a parsec-scale tori, postulated to exist in Seyfert galaxies (e.g., Antonucci & Miller 1985; Krolik & Begelman 1986), then such a photon field may be important (e.g., Sikora et al. 1994). These photons can be emitted from the dust around the nucleus but may be hidden by the strong jet emission in the observer's frame; in fact, our spectrum (see Fig. 4) does not exclude such emission. We can easily predict that if the total luminosity of such IR photons exceeds $L_{dust} \gtrsim 10^{43}$ ergs s^{-1}, it can contribute sufficient seed photons that subsequently would be Comptonized to dominate the TeV spectrum. The precise (subarcsec) IR/optical imaging of Mrk 501 should limit the spatial extent of the "IR-bump" mentioned above.

The second possible cause of the TeV spectral discrepancy is the contribution of photons produced by multiple

Compton scattering (e.g., Band & Grindlay 1985, 1986; Bloom & Marscher 1996). In considering the second-order scattering, the same formula (2) is used, except that the incident photons are now the first-order inverse Compton photon density (Bloom & Marscher 1996). Our calculation shows the contribution from multiple Compton scattering is greatly suppressed owing to the Klein-Nishina effect. The flux ratio for Comptonization of first and second order is $f_{2nd}/f_{1st} \lesssim 10^{-3}$ at 1 TeV. Thus, the second order SSC process does not make a significant contribution to the spectrum, and we are unable to explain the relatively flat TeV spectrum in 1996 March.

A beaming factor much larger than 10 could also make TeV spectrum flatter. However, our previous calculation shows that at $\delta \gtrsim 40$, Compton cooling time for highly energetic electrons becomes larger than the source crossing timescale R/c, and thus no clear break should appear in the electron population. Also, a beaming factor much larger than 10 (e.g., $\delta \gtrsim 100$) does not reproduce the GeV/TeV flux ratio of $f_{EGRET}/f_{Whipple} \sim 10$, but it makes both fluxes comparable because most of the scattering will take place in the Thomson regime.

Although the boundary for the allowed parameter space could be changed if variability on shorter timescales is found (see Fig. 5), a more tightly constrained TeV spectral index (through better statistics and less systematic error) will be of great value to make further progress on modeling of this source. Together with more refined SSC models such as Marscher (1980) and Ghisellini & Maraschi (1989), we have shown that an exact evaluation of Comptonized emission from external IR photons, such as dust emission around the nuclei and accretion disk photons, may be useful for the understanding of the origin of the flat TeV spectrum. Our model here is constructed with no time dependence. To be exact, this model should be expanded to include the full time-dependent evolution of the electron and photon spectra (e.g., Mastichiadis & Kirk 1997). The time dependent treatment for Mrk 501 flare will be discussed elsewhere.

5. CONCLUSION

We conducted a multiwavelength campaign for the TeV blazar Mrk 501 in 1996 March. In the EGRET data, we found 3.5 σ detection ($E > 100$ MeV) of high-energy γ-rays. Higher flux was also observed in 1996 April and May, with 4.0 σ significance for $E > 100$ MeV and 5.2 σ significance for $E > 500$ MeV. The maximum flux observed with *ASCA* was 5 times higher than the quiescent level and gradually decreased by a factor of 2 as the spectrum steepened. The spectra obtained with *ASCA* show a "break" around 2 keV, which is interpreted as the peak of the synchrotron emission. Comparing our results with the observations in 1997 April, there were notable changes in overall spectra, such as a 2 decade shift of the peak frequency of the synchrotron component, a change of peak flux in the keV region by a factor of 9, and a flux change in the TeV region by a factor of 33. To investigate a correlated variation of spectra in the keV and TeV region, we applied a one-zone, homogeneous SSC model with an electron distribution having two break points. The allowed parameter space (B, δ) was systematically investigated to obtain values for the model parameters. The spectrum in 1996 March was consistent with parameters $\gamma_{max} = 1.8 \times 10^6$, $B = 0.2$ gauss, $\delta = 15$, and $R = 4.5 \times 10^{15}$ cm. The correlation of the

keV/TeV flare amplitudes in 1997 April was also reproduced with the assumption that an additional electron population, with higher maximum energies ($\gamma_{max} \sim 6 \times 10^6$), was newly injected and scattered the photons emitted from the steady component, assumed to be the same level as that in 1996. We found that the scattering of the synchrotron photons emitted from only the flare electron population is inadequate in our model. The flat TeV spectrum observed with HEGRA in 1996 March is discrepant with our model. We considered the contribution from the galactic IR photons and higher order Comptonization, and found that neither could make the TeV spectrum flatter. A possible contribution from the parsec-scale tori, postulated to exist in Seyfert galaxies, was also investigated. We need better quality data, especially in the hard X-ray and γ-ray regimes, to better understand the emission mechanism. Observations with a next generation of satellites, featuring improved sensitivity at hard X-ray/γ-ray energies, such as *Astro–E* and *GLAST*, are expected to bring valuable information.

REFERENCES

Aharonian, F., et al. 1997, A&A, 327, L5
Antonucci, R., & Miller, J. 1985, ApJ, 297, 621
Band, D. L., & Grindlay, J. E. 1985, ApJ, 298, 128
———. 1986, ApJ, 308, 576
Bednarek, W., & Protheroe, R. J. 1997, MNRAS, 292, 646
Binney, J., & Tremaine, S. 1987, Galactic Dynamics (Princeton: Princeton Univ. Press)
Bloom, S. D., & Marscher, A. P. 1996, ApJ, 461, 657
Blumenthal, G. R., & Gould, R. J. 1970, Rev. Mod. Phys., 42, 237
Bradbury, S. M., et al. 1997, A&A, 320, L5
Buckley, J. H., et al. 1996, ApJ, 472, L9
Burke, B. E., et al. 1991, IEEE Trans. ED 38, 1069
Catanese, M., et al. 1997, ApJ, 487, L143
———. 1998, ApJ, 501, 616
Cawley, M. F., & Weekes, T. C. 1995, Exp. Astron., 6, 7
Comastri, A., et al. 1997, ApJ, 480, 534
Dermer, C. D. 1995, ApJ, 446, L63
Dermer, C. D., & Schlickeiser, R. 1993, ApJ, 416, 458
Dermer, C. D., Stauner, S. J., & Schlickeiser, R. 1997, ApJS, 109, 103
Elvis, M., et al. 1989, AJ, 97, 777
Falomo, R., et al. 1993, AJ, 106, 11
Fichtel, C. E., et al. 1994, ApJS, 94, 551
Gaidos, J. A., et al. 1996, Nature, 383, 319
George, I. M., Warrick, R. S., & Bromage, G. E. 1988, MNRAS, 232, 793
Ghisellini, G., & Maraschi, L. 1989, ApJ, 340, 181
Giommi, P., et al. 1990, ApJ, 356, 432
Gould, R. J., et al. 1979, A&A, 76, 306
Hillas, A. M., et al. 1998, ApJ, 503, 744
Inoue, S., & Takahara, F. 1996, ApJ, 463, 555
Jones, F. C. 1968, Phys. Rev., 167, 1159
Jones, T. W., O'Dell, S. L., & Stein, W. A. 1974, ApJ, 188, 353
Kirk, J. G., Rieger, F. M., & Mastichiadis, A. 1998, A&A, 333, 452
Königl, A. 1981, ApJ, 243, 700

Kubo, H., et al. 1998, ApJ, 504, 693
Krolik, J., & Begelman, M. 1986, ApJ, 308, L55
Macomb, D., et al. 1995, ApJ, 449, L99
Makino, F., Fink, H. H., & Clavel, J. 1992, in Frontiers of X-ray Astronomy, ed. Y. Tanaka & K. Koyama (Tokyo: Universal Academy)
Maraschi, L., Ghisellini, G., & Celotti, A. 1992, ApJ, 397, L5
Marscher, A. P. 1980, ApJ, 235, 386
Marscher, A. P., & Gear, W. K. 1985, ApJ, 298, 114
Marscher, A. P., & Travis, J. P. 1996, A&AS, 120, 537
Mastichiadis, A., & Kirk, J. G. 1997, A&A, 320, 19
Mattox, J. R., et al. 1993, ApJ, 410, 609
———. 1996, ApJ, 461, 396
———. 1997a, ApJ, 476, 692
———. 1997b, ApJ, 481, 95
Mukherjee, R., et al. 1997, ApJ, 490, 116
Ohashi, T., et al. 1996, PASJ, 48, 157
Petry, D. 1997, Ph.D. thesis, Max-Planck-Institute for Physics, Munich
Petry, D., et al. 1996, A&A, 311, L13
Pian, E., et al. 1998, ApJ, 492, L17
Press, W. H., et al. 1992, Numerical Recipes in C (Cambridge: Cambridge Univ. Press)
Punch, M., et al. 1992, Nature, 358, 477
Quinn, J., et al. 1996, ApJ, 456, L83
———. 1999, in preparation
Sikora, M., Begelman, M. C., & Rees, M. J. 1994, ApJ, 421, 153
Sreekumar, P., et al. 1998, ApJ, 494, 523
Takahashi, T., et al. 1996a, ApJ, 470, L89
———. 1996b, Mem. Soc. Astron. Italiana, 67, 533
Thompson, D. J., et al. 1993, ApJS, 86, 629
———. 1995, ApJS, 101, 259
Ulrich, M.-H., Maraschi, L., & Urry, C. M. 1997, ARAA, 35, 445
von Montigny, C., et al. 1995, ApJ, 440, 525
Weekes, T. C., et al. 1996, A&AS, 120, 603